THE JOURNAL OF PHYSICAL CHEMISTRY B
A JOURNAL OF THE AMERICAN CHEMICAL SOCIETY

pubs.acs.org/JPCB

Article

Interfacial Water Structure of Binary Liquid Mixtures Reflects Nonideal Behavior

Published as part of The Journal of Physical Chemistry virtual special issue "Dor Ben-Amotz Festschrift".

Xiaoqing Yu,[#] Takakazu Seki,[#] Chun-Chieh Yu, Kai Zhong, Shumei Sun, Masanari Okuno, Ellen H. G. Backus, Johannes Hunger, Mischa Bonn,[*] and Yuki Nagata[*]

Cite This: *J. Phys. Chem. B* 2021, 125, 10639−10646

Read Online

ACCESS | Metrics & More | Article Recommendations | Supporting Information

ABSTRACT: The evaporation of molecules from water−organic solute binary mixtures is key for both atmospheric and industrial processes such as aerosol formation and distillation. Deviations from ideal evaporation energetics can be assigned to intermolecular interactions in solution, yet evaporation occurs from the interface, and the poorly understood interfacial, rather than the bulk, structure of binary mixtures affects evaporation kinetics. Here we determine the interfacial structure of nonideal binary mixtures of water with methanol, ethanol, and formic acid, by combining surface-specific vibrational spectroscopy with molecular dynamics simulations. We find that the free, dangling OH groups at the interfaces of these differently behaving nonideal mixtures are essentially indistinguishable. In contrast, the ordering of hydrogen-bonded interfacial water molecules differs substantially at these three interfaces. Specifically, the interfacial water molecules become more disordered (ordered) in mixtures with methanol and ethanol (formic acid), showing higher (lower) vapor pressure than that predicted by Raoult's law.

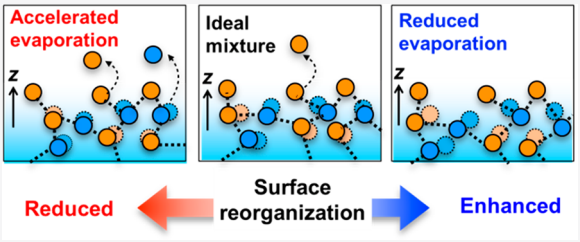

I. INTRODUCTION

Binary liquid mixtures typically deviate from ideal mixing in a thermodynamic context.[1,2] In the bulk liquid phase, such nonideal interactions can be trivially understood, as they only require, in a mixture of A and B species, that the interactions between A and B differ from A−A and B−B interactions. A textbook example for nonideal mixtures where A−B interactions are stronger than A−A and B−B interactions in water−formic acid mixtures.[3] As a result, the vapor pressure of water−formic acid mixtures is markedly lower than that predicted by Raoult's law. Conversely, water−alcohol mixtures typically show excess vapor pressures.[4] These excess interactions impact the energetics of the evaporation, which is directly relevant to distillation and purification processes in industrial processes and also to atmospheric processes.[5−11]

While these energetics have been traced to the intermolecular interactions in the bulk, evaporation takes place at the interface and molecular interactions[12] and the abundancy of the molecules at the interface are decisive factors determining evaporation rates. The activation barrier for the evaporation process and thus evaporation rate of an ideal A−B liquid binary mixture vary linearly with the concentration of A and B species, when A−A, A−B, and B−B interactions are identical, as defined in Raoult's law. However, also the evaporation kinetics of real, nonideal mixtures show deviations from this simple rule.[13−15] For example, the evaporation rate $k_{H_2O-Ethanol}(x_{H_2O})$ of the water−ethanol mixture at a water concentration of x_{H_2O} is higher than the rate predicted from the linear combination of the rates of pure water (k_{H_2O}) and pure ethanol ($k_{Ethanol}$): $k_{H_2O-Ethanol}(x_{H_2O}) > x_{H_2O}k_{H_2O} + (1 - x_{H_2O})k_{Ethanol}$, where x_{H_2O} denotes the mole fraction of water. In turn, the water−formic acid mixture shows the opposite trend (Figure 1a, see the Supporting Information for more details). Although these differences in the evaporation rates largely reflect the evaporation energetics (i.e., the respective vapor pressures as shown in Figure 1b),[16] the impact of the different intermolecular interactions in the bulk liquid on the molecular conformation and ordering at the interface of these binary mixtures—highly relevant to evaporation kinetics—has been poorly understood. Figure 1 illustrates that the nonideal behavior is complex: not only do the mixtures exhibit different deviations from ideality, but there is also a strong asymmetry with respect to the molar composition. For instance, for the water−ethanol mixture, the maximum deviation of the vapor pressure occurs at $x_{H_2O} = 0.85$, while the excess evaporation rate peaks at lower values of x_{H_2O}. The following question

Received: July 5, 2021
Revised: August 21, 2021
Published: September 10, 2021

https://doi.org/10.1021/acs.jpcb.1c06001
J. Phys. Chem. B 2021, 125, 10639−10646

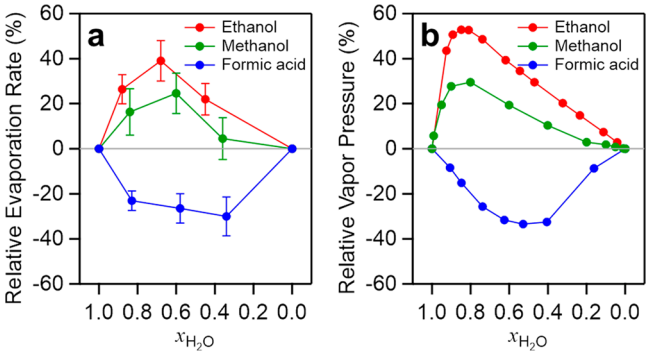

Figure 1. (a) Relative evaporation rate obtained from aqueous binary mixtures of methanol, ethanol, and formic acid vs water mole fraction, x_{H_2O}. The relative evaporation rate was calculated via $\Delta k(x_{H_2O}) = k_{H_2O-org}(x_{H_2O})/k_{pred}(x_{H_2O}) - 1$, where $k_{H_2O-org}(x_{H_2O})$ is the measured evaporation rate of the binary mixture and $k_{pred}(x_{H_2O})$ is the predicted evaporation rate from the evaporation rate of pure water (k_{H_2O}) and pure organic species (k_{org}): $k_{pred}(x_{H_2O}) = x_{H_2O}k_{H_2O} + (1 - x_{H_2O})k_{org}$. The error bar indicates the 95% confidence interval of the measured evaporation rate. (b) Relative vapor pressure for the binary mixtures at 333 K. The data were calculated via $\Delta p(x_{H_2O}) = p_{H_2O-org}(x_{H_2O})/p_{pred}(x_{H_2O}) - 1$, where $p_{H_2O-org}(x_{H_2O})$ is real vapor pressure[3,4,29] and $p_{pred}(x_{H_2O})$ is the predicted one from Raoult's law. See the Supporting Information for more details.

presents itself: What is happening at the surface of the liquid mixture?

Here, we explore the molecular conformations of aqueous binary mixtures using surface-specific vibrational sum-frequency generation (SFG) spectroscopy. This technique can uniquely probe molecules within a few surface layers through their vibrational response.[17,18] In fact, SFG spectroscopy has already been applied to probe the interfacial structure of various binary liquid mixtures, including water−methanol,[19−23] water−ethanol,[21,24,25] and water−formic acid[26] mixtures probing the O−H stretching mode. However, because these organic species commonly contain O−H groups, SFG spectra in the O−H stretching mode region cannot distinguish both molecular species individually. This challenge can be circumvented by probing the water bending mode, which allows disentangling the water contribution from other vibrational modes such as the C−O−H bending mode of the organic species.[27,28] However, for aqueous alcohol or formic acid mixtures, the water structure at the interface has not been isolated.

By combining SFG spectroscopy with molecular dynamics (MD) simulations, we determine the interfacial structure and correlate the interfacial structure with evaporation thermodynamics and kinetics for binary mixtures of water with methanol/ethanol/formic acid. We found that the variations of the C−H stretching mode of organic species and the free O−H stretching mode of water upon the addition of the organic species do not show a significant difference between the aqueous binary mixtures of methanol, ethanol, and formic acid. In contrast, the H−O−H bending mode of water in these mixtures differs substantially. The spectra and MD simulation results reveal that water's interfacial alignment becomes randomized upon adding ethanol and methanol to water, while it becomes ordered upon adding formic acid. Our results thus show that the nonideal interaction in bulk is reflected in the structure of water at the interface, relevant to the evaporation rates.

II. METHODS

II.A. Sample Preparation. The mixtures were prepared using methanol (HPLC, gradient grade, ≥99.8% (GC), <0.01% water, VWR International), ethanol (Puriss., absolute, ≥99.8% (GC), Sigma-Aldrich), formic acid (Suprapur, 98−100% (ACS), Merck KGaA), D_2O (99.9 atom % D, Sigma-Aldrich), and Milli-Q water (18.2 MΩ cm). All substances were used without further purification. To avoid the overlap between the C═O stretching mode (~1720 cm^{-1})[26] and the H−O−H bending mode (~1650−1750 cm^{-1}),[28] we measure the H−O−D bending region for the water−formic acid system. We prepared samples using H_2O:D_2O mixtures and formic acid. We used 1:1 H_2O:D_2O mixtures for samples with formic acid mole fractions of 0, 0.02, 0.08, 0.14, and 0.32. 1:3 H_2O:D_2O mixtures and pure D_2O were used for formic acid mole fractions of 0.53 and 0.66, respectively. The determination of x_{HOD} is given in the Supporting Information. The aqueous binary mixtures were contained in a trough with a diameter of 5 cm for the SFG measurements.

II.B. SFG Measurements. The SFG measurements for the free O−H stretching mode and H−O−H/H−O−D bending mode of all of the aqueous binary mixtures as well as the C−H stretching mode of water−methanol mixtures used a femtosecond Ti:sapphire amplified laser system (Coherent Libra, ~800 nm, ~50 fs, 1 kHz) with 5 W output power. We used 2 W to pump an optical parametric amplifier (TOPAS, light conversion) with a non-collinear difference frequency generation stage to generate a broadband IR pulse. Another 1 W of the laser output was passed through an etalon to generate a narrowband visible pulse (~20 cm^{-1}). The incident angles of the visible and IR beams were 64 and 40° with respect to the surface normal, respectively. The visible (20 μJ) and IR (1 μJ) pulses were overlapped spatially and temporally at the sample position. Subsequently, the generated SFG signal was dispersed in a spectrometer (Shamrock 303i, Andor Technology) and detected by an EMCCD camera (Newton, Andor Technology).

For the C−H stretching mode of water−ethanol and water−formic acid mixtures, the experiments were carried out with a femtosecond Ti:sapphire amplified laser system (Spitfire Ace, Spectra-Physics, ~800 nm, ~40 fs, 1 kHz) with 5 W output power. The visible (13 μJ) and IR (5 μJ) incident angles were 36 and 41°, respectively. The generated SFG pulse was subsequently guided into a spectrograph (Acton SP 300i, Princeton Instruments) and detected with an EMCCD (Newton, Andor Technology).

The C−H stretching mode and the free O−H stretching mode signals were recorded twice for 3 min at the air−aqueous binary mixture interfaces. For water−alcohol mixtures, we measured the H−O−H bending mode signals twice for 10−15 min at the air−solution interface. For water−formic acid mixtures, the H−O−D bending mode was measured in a similar manner to the H−O−H bending mode. To avoid IR absorption of water vapor, we purged N_2 for 10 min for the measurements of the free O−H stretching mode and the H−O−H/H−O−D bending mode. All spectra were collected in the ssp (denoting s-, s-, and p-polarized SFG, visible, and IR, respectively) polarization combination. The spectra for the air−binary mixture interfaces were normalized to the non-

https://doi.org/10.1021/acs.jpcb.1c06001
J. Phys. Chem. B 2021, 125, 10639−10646

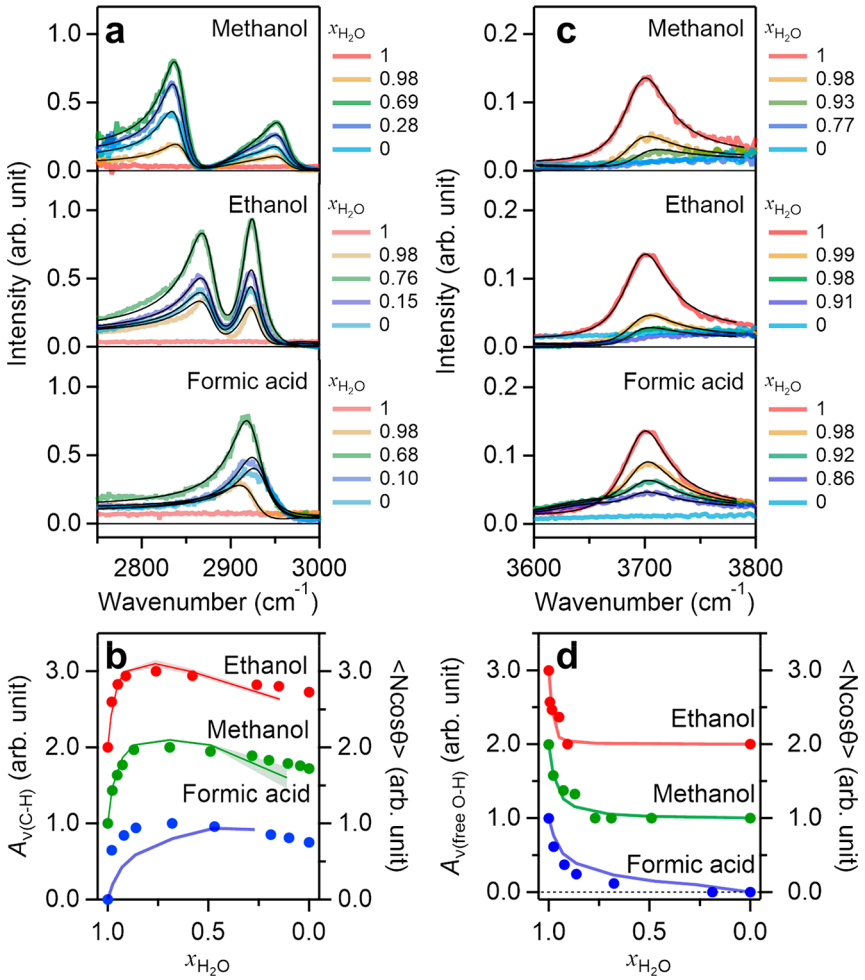

Figure 2. (a) The C−H stretching mode SFG spectra at the air−aqueous binary mixture of methanol, ethanol, and formic acid interfaces. The black lines represent the fits to the SFG spectra. (b) The variations of the amplitudes for the C−H symmetric stretching mode peak of methanol and ethanol CH_3 group as well as for the C−H stretching mode peak of formic acid together with the simulation data of integrated $\langle N \cos\theta \rangle$ (solid lines). (c) The free O−H stretching mode SFG spectra at the air−aqueous mixture interfaces. The black lines represent the fits to the SFG spectra. (d) The variation of $A_{\nu(\text{free O−H})}$ with composition together with the simulation data of integrated $\langle N \cos\theta \rangle$ (solid lines). Data for different mixtures in parts b and d are normalized to the maximum amplitude and offset by increments of 1 for clarity.

resonant signal taken from *z*-cut quartz after subtracting a background spectrum.

II.C. MD Simulation Protocols. We carried out the MD simulation for the air−aqueous binary mixture interfaces in the slab geometry. We used the GROMACS software for performing the MD simulations.[30] For the aqueous binary mixture, we used the OPLS-AA force field model[31] for methanol and ethanol, the modified OPLS-AA model for formic acid, and the TIP4P/2005 model for water.[32] The simulation cell was 26.6 Å × 26.6 Å × 350 Å with the periodic boundary condition. We obtained more than 100 ns trajectories, from which we computed the orientation of water in aqueous binary mixtures. The details of the simulation can be found in the Supporting Information.

We evaluated the orientations of the water molecules located in the interfacial region. The interfacial region is defined as $|z - z_G| < a$, where z is the z-coordinate of the oxygen atom of a water molecule, z_G is the position of the Gibbs dividing surface for the mixtures, and a^3 represents the average volume occupied by a molecule in the liquid phase. Here, the z-axis forms the surface normal.

III. RESULTS AND DISCUSSION

III.A. Variations of the C−H and Free O−H Stretching Modes at the Air−Binary Mixture Interfaces. We explore the interfacial organization of the organic components at the air−aqueous binary mixture interfaces by probing the C−H stretching mode ν(C−H) of methanol/ethanol/formic acid with SFG spectroscopy. The measured SFG signal is determined by the average molecular orientation and proportional to the number of interfacial molecules contributing to the signal. Figure 2a displays the ν(C−H) SFG spectra with various mixture concentrations. All of the data except for pure H_2O show clear C−H stretching mode peaks, reflecting that the hydrophobic groups of the topmost methanol/ethanol/formic acid molecules point out of the liquid phase. The SFG spectra at the air−aqueous binary mixture of the methanol interface show peaks at 2840 and 2960 cm^{-1} and a shoulder at 2930 cm^{-1}, which are assigned to the symmetric C−H stretching mode, the antisymmetric C−H stretching mode, and the Fermi resonance of the C−H stretching and C−H bending modes, respectively.[33−35] Despite earlier assignments to the Fermi resonance,[20] a recent study provides evidence for the ∼2960 cm^{-1} band to be due to the antisymmetric CH_3

https://doi.org/10.1021/acs.jpcb.1c06001
J. Phys. Chem. B 2021, 125, 10639−10646

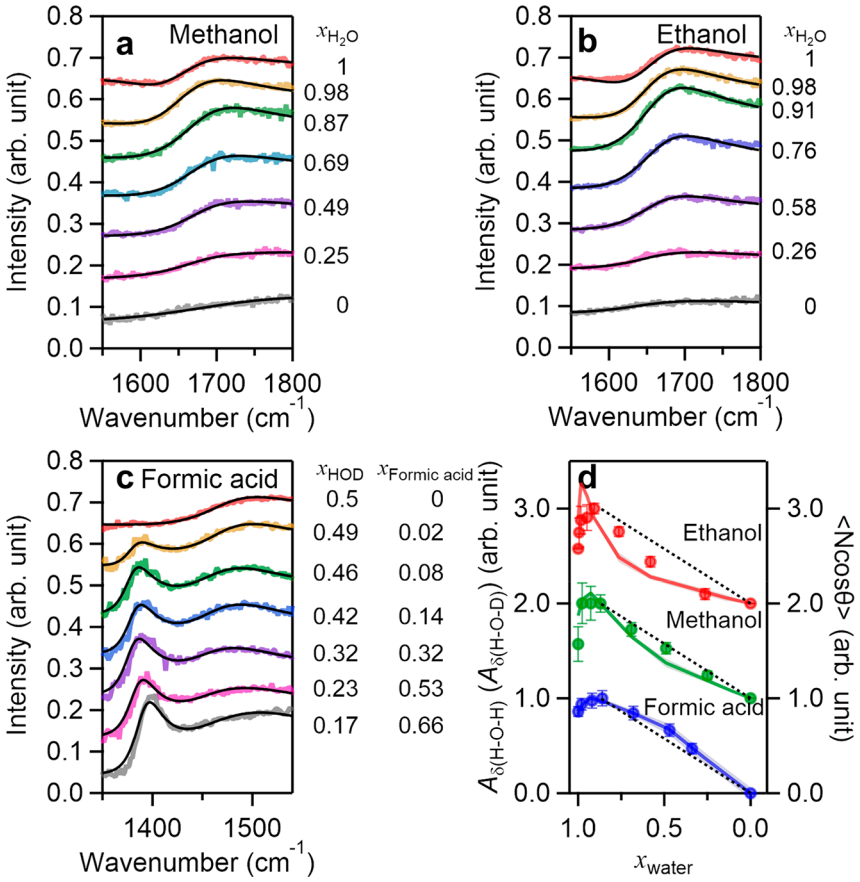

Figure 3. (a–c) SFG spectra at the air–aqueous binary mixture of (a) methanol, (b) ethanol, and (c) formic acid interfaces. Spectra are offset by 0.1 for clarity. The black lines represent the fits to the SFG spectra. (d) $A_{\delta(H-O-H)}$ for the water–methanol and water–ethanol mixtures together with $A_{\delta(H-O-D)}$ for the water–formic acid mixture. $A_{\delta(H-O-H)}$ and $A_{\delta(H-O-D)}$ were normalized to the values at x_{H_2O} of ∼0.85, where the free O–H stretching mode contributions ($A_{\nu(\text{free O–H})}$) become vanishingly small. For mixtures with formic acid, x_{water} corresponds to the fraction of all water species (x_{H_2O} + x_{HOD} + x_{D_2O}). The error bars are obtained from the fits. The solid lines indicate the simulation data of integrated $\langle N \cos\theta \rangle$; the dashed lines connect the extrema of the measurements at x_{H_2O} = 0 and 0.85. Data for different mixtures are offset by increments of 1 for clarity.

stretching mode.[33] For the interface of the water–ethanol mixtures, the 2876 cm^{-1} Fermi resonance and the 2924 cm^{-1} symmetric C–H stretching mode of the CH_3 group govern the SFG spectra in the C–H range,[36] while the 2970 cm^{-1} antisymmetric C–H stretching mode and the C–H stretching mode of the CH_2 groups are weak—in line with a previous study.[20] At the interface of the aqueous binary mixture of formic acid with air, a single peak is observed at 2930 cm^{-1}, which arises from the C–H stretching mode of formic acid.[26] The frequency shift of the C–H stretching peak with varying water concentration is attributed to cis-/trans-conformations of the formic acid.[37]

To quantify the changes in the spectra, we fit the data with a Lorentzian line shape model, and the obtained fit curves are represented by solid black lines in Figure 2a. We plot the inferred amplitude of the symmetric C–H stretching mode of the CH_3 group for methanol/ethanol and the C–H stretching mode for formic acid ($A_{\nu(C-H)}$) in Figure 2b (see the Supporting Information). All mixtures have in common that the C–H stretching mode contribution increases steeply with decreasing x_{H_2O} from 1 to ∼0.7, while it starts to decrease when x_{H_2O} decreases below 0.7. The turnover behavior of $A_{\nu(C-H)}$ is consistent with previous studies,[19,21,38−40] indicative of randomization of the C–H groups,[22] with decreasing water concentration in the binary mixtures.

We then investigated the structure of the topmost O–H groups. We measure the free O–H stretching mode (ν(free O–H)) SFG features at the air–aqueous binary mixture interfaces, which allows quantifying the number of non-hydrogen-bonded, free O–H groups at the interface. We note that these experiments require purging with N_2 to exclude water vapor, yet the effect of purging on the C–H stretching mode is negligible (Supporting Information) and our spectra reflect the equilibrium interfacial composition. The measured spectra displayed in Figure 2c show that the free O–H stretching peak is centered at 3700 cm^{-1} [41] for all mixtures and vanishes quickly upon the addition of methanol/ethanol/formic acid. To quantify these trends, we determine the amplitudes of the free O–H peak, $A_{\nu(\text{free O–H})}$ (Figure 2d and the Supporting Information). These amplitudes indicate that the free O–H contribution decreases rapidly with decreasing x_{H_2O} and approaches zero already for x_{H_2O} = 0.85. Also, this observation is consistent with previous studies.[26,42]

The variations of the C–H and free O–H stretching modes are consistent with MD simulation data. From the MD result, we calculated the angle θ of the transition dipole moment orientation of symmetric C–H stretching modes of methanol and ethanol as well as the C–H stretching mode of formic acid

https://doi.org/10.1021/acs.jpcb.1c06001
J. Phys. Chem. B 2021, 125, 10639−10646

with respect to the surface normal. The MD simulations also provide access to the number of (symmetric) C−H or O−H stretching chromophores N. The SFG spectral amplitude is approximately proportional to $\langle N \cos\theta \rangle$, allowing us to compare the simulation data with the experimental data. Parts b and d of Figure 2 show $\langle N \cos\theta \rangle$ for, respectively, the symmetric C−H stretching modes and the free O−H chromophores. The good agreement between the simulation and experiment in Figure 2b and d supports the notion that the turnover behavior of the variations of the C−H and steep decrease of free O−H stretching contributions arise from the interfacial structure change of the binary mixtures upon the addition of methanol/ethanol/formic acid.[22]

The decrease in the free O−H stretching mode contribution together with the increase in the C−H stretching mode contribution with decreasing x_{H_2O} suggests that the addition of the organic solutes results in hydrogen-bond formation of the organic solute to water's free O−H groups already at very low solute concentrations in the aqueous binary mixtures. Remarkably, the variations of the two molecular groups sticking out of the interfaces, the C−H groups and the free O−H group, behave very similarly for all three aqueous binary mixtures, irrespective of their very different excess mixing properties and the different excess evaporation rates for water−ethanol and water−methanol mixtures compared to water−formic acid mixtures. As such, based on these observations, the interfacial structures as determined from the groups pointing toward air appear similar for all three mixtures. However, the question of whether the different mixing behavior is reflected in the hydrogen-bonded structure of water at the interface remains.

III.B. Orientation of the Interfacial Water Molecules Viewed through the Water Bending Mode. To study interfacial hydrogen-bonded water, one may consider using SFG spectroscopy to probe the hydrogen-bonded O−H stretching mode region. However, as noted in the Introduction, the SFG signal from the O−H stretching modes of hydrogen-bonded water molecules cannot be disentangled from the signal from the O−H groups of methanol/ethanol/formic acid (see the Supporting Information). Moreover, vibrational couplings markedly alter the line shape of the O−H stretching band.[43] In contrast, the H−O−H bending mode signal arises solely from water and contains no contributions from methanol/ethanol/formic acid. What is more, the line shape of the water bending mode is rather insensitive to intermolecular coupling,[27,44] making it ideal for probing interfacial water.[45]

In Figure 3a and b, we show the measured H−O−H bending mode (δ(H−O−H)) spectra of H_2O−methanol and H_2O−ethanol mixtures, respectively. The spectrum for the air−neat water interface ($x_{H_2O} = 1$) shows a dip at ∼1612 cm^{-1} and a broad bending mode band at 1650−1750 cm^{-1}.[28,46−48] These spectral features are assigned, respectively, to up-oriented water molecules donating one hydrogen bond (the other O−H is free) and to down-oriented water molecules donating two hydrogen bonds (termed bend 1 and bend 2 in the Supporting Information). For mixtures with formic acid, we use the H−O−D bending mode of H_2O/D_2O mixtures rather than the H−O−H bending mode because the C═O stretching mode (∼1720 cm^{-1})[26] partly overlaps and interferes with the H−O−H bending mode (∼1660 cm^{-1}) (see the Supporting Information). Figure 3c displays the H−O−D bending mode (δ(H−O−D)) spectra of the isotopically diluted water−formic acid mixture. The H−O−D bending mode frequency is red-shifted by ∼200 cm^{-1} compared to the H−O−H bending mode frequency.[27] When formic acid is added to water, the C−H bending mode (∼1350−1400 cm^{-1})[49−52] and the C−O−H bending mode (∼1490 cm^{-1})[53,54] appear as features in this frequency region together with the H−O−D bending mode contribution (∼1460 cm^{-1}).

We extracted the composition-dependent amplitudes by fitting a Lorentzian model (see the Supporting Information) using two bands to the bending mode data. These two bands have been attributed to water molecules that form one hydrogen bond and the other O−H group being a free O−H group and to water molecules whose O−H groups are both pointing into the liquid and are both hydrogen-bonded. Figure 3d displays the variation of the sum of these amplitudes for the H−O−H and H−O−D bending mode amplitudes ($A_{\delta(H-O-H)}$ and $A_{\delta(H-O-D)}$). As already apparent from the raw data, the water response initially increases with increasing concentration of the organic solute, showing a maximum at $x_{H_2O} = 0.85$, after which the band decreases in intensity. The initial increase coincides with the disappearance of the free O−H stretching contribution at x_{water} between 1.0 and ∼0.85 (Figure 2d). As such, the initial increase can be ascribed to an increase in the number of doubly H-bond donating water molecules at the interface: the water molecules with a free O−H group reorient to have both O−H groups pointing into the bulk liquid.

Unlike the data in Figure 2, which showed similar behavior for the three mixtures, the variation of $A_{\delta(H-O-H)}$ and $A_{\delta(H-O-D)}$ with composition differs markedly for $x_{water} < 0.85$ for the three mixtures. To better illustrate these differences, we normalize the bending mode amplitudes in Figure 3d to the maximum amplitude at $x_{water} = 0.85$ at which the free O−H contribution has vanished and the associated rotation of water molecules hardly affects the bending mode amplitudes and connect that to the zero signal at $x_{water} = 0$ (dashed lines in Figure 3d). For the water−methanol and water−ethanol mixtures, $A_{\delta(H-O-H)}$ is, respectively, moderately and significantly below this line; for the water−formic acid mixture at $x_{water} < 0.85$, the results lie above the line (Figure 3d). As such, our results demonstrate positive (negative) excess spectral amplitude for the water bending vibration in mixtures with formic acid (methanol and ethanol) at $x_{water} < 0.85$. These excess spectral amplitudes of water correlate with the evaporation energetics and kinetics: Mixtures exhibiting a positive excess evaporation rate and vapor pressure exhibit reduced spectral amplitudes.

The negative and positive excess spectral amplitudes for the bending mode are indicative of different degrees of ordering of interfacial water for the different mixtures, with the larger signal for formic acid implying more ordered water. We test this hypothesis by performing MD simulations and calculate the angle θ of the H−O−H angular bisector with respect to the surface normal for hydrogen-bonded water molecules at the interface. By calculating the integrated $\langle N \cos\theta \rangle$ along the surface normal, where N is the number of water molecules, one can compare the simulation data of $\langle N \cos\theta \rangle$ with the experimental data of $A_{\delta(H-O-H)}$ or $A_{\delta(H-O-D)}$. The result is shown as solid lines in Figure 3d, demonstrating good agreement with the experimental data. Clearly, the MD simulations capture the variation of the interfacial water response.

https://doi.org/10.1021/acs.jpcb.1c06001
J. Phys. Chem. B 2021, 125, 10639−10646

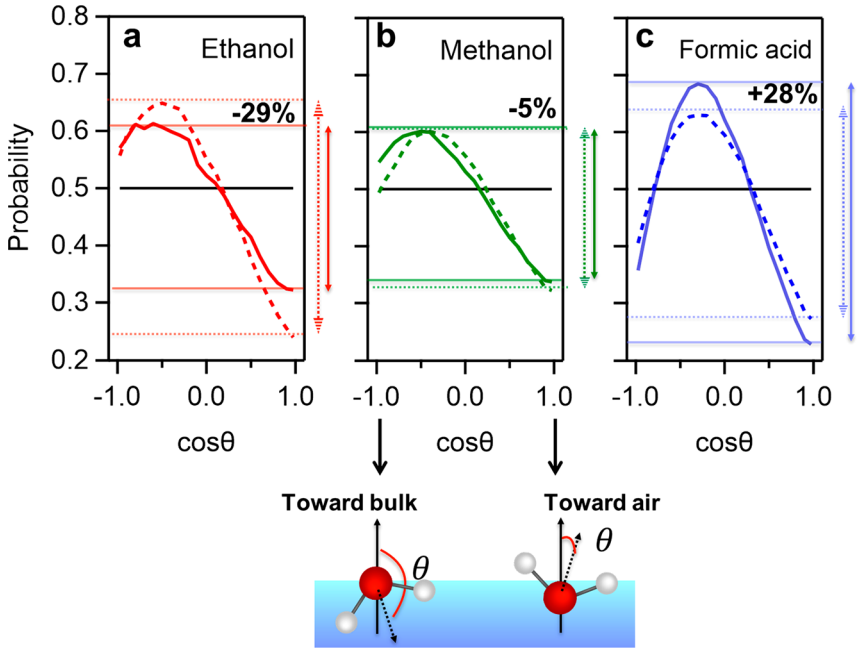

Figure 4. (a–c) The cos θ distribution probability of the angular H–O–H bisector of the interfacial water for x_{H_2O} = 0.5 (solid lines) and 0.85 (dotted lines) for the aqueous binary mixtures of (a) ethanol, (b) methanol, and (c) formic acid. The horizontal black lines reflect a totally randomized distribution; the arrows indicate the variations of maximum (Max($P_{x_{H2O}}$)) and minimum (Min($P_{x_{H2O}}$)) ranges of the cos θ distribution. The percentages given in the figures indicate the relative change of these ranges, $[(\mathrm{Max}(P_{0.5}) - \mathrm{Min}(P_{0.5})) - (\mathrm{Max}(P_{0.85}) - \mathrm{Min}(P_{0.85}))]/[\mathrm{Max}(P_{0.85}) - \mathrm{Min}(P_{0.85})]$.

The reduced (increased) $\langle N \cos\theta \rangle$ values (and spectral amplitudes $A_{\delta(\mathrm{H-O-H})}$ or $A_{\delta(\mathrm{H-O-D})}$) may stem from a reduced (increased) interfacial water density (N) or reduced (enhanced) water alignment ($\langle \cos\theta \rangle$). Our MD simulation data show that the variations of the spectral amplitudes are caused by reduced (enhanced) water alignment: At $x_{H_2O} \sim 0.85$ (dotted line in Figure 4a–c), where rotation due to hydrogen-bond formation of initially free O–H groups is completed (see the discussion above), the widths of the distributions of ethanol and formic acid are similar. However, for ethanol, it is centered at larger angles ($\langle \cos\theta \rangle = -0.5$), as compared to formic acid ($\langle \cos\theta \rangle = -0.3$). The orientational distribution in mixtures with methanol is much broader and centered at $\langle \cos\theta \rangle = -0.4$. These trends are enhanced upon increasing the solute concentration to $x_{H_2O} \sim 0.5$: For the ethanol sample, the cos θ distribution of the angular H–O–H bisector direction broadens upon the addition of ethanol, which means that the orientation of water is further randomized. The distributions for methanol are similar to ethanol, yet the variation of the distribution upon increasing methanol content is smaller than that for ethanol. In contrast to the methanol/ethanol samples, the distribution of water orientations in the presence of formic acid becomes more narrow upon increasing the formic acid concentration. As such, the simulation results demonstrate an enhanced alignment of water upon mixing with formic acid, slightly disordered water for methanol, and substantially disordered water for ethanol.

Our results, therefore, show that the different excess mixing properties in the bulk liquids result in markedly different structuring of water for these mixtures at the interface. The deviations from Raoult's law point to stronger (weaker) solute–water interactions as compared to water–water interactions for formic acid (methanol and ethanol), leading to stronger (weaker) constraints on the orientation of water. Interestingly, the stronger solute–water interactions for formic acid lead to enhanced ordering of interfacial water, and the sample shows reduced evaporation rates. Inversely, when the degree of the surface organization is reduced, i.e., the surface structure becomes more randomized, as is seen upon the addition of ethanol to water, the sample shows an excessive evaporation rate.

IV. CONCLUSION

We performed surface-specific vibrational SFG spectroscopy and MD simulations for the air–aqueous binary mixture interfaces of ethanol, methanol, and formic acid to explore their surface molecular conformations. Despite the largely differing excess mixing properties of the three studied mixtures, the variation of the outermost arrangement judged by the presence of spectral signatures of free O–H groups and the C–H stretching mode is similar for all three mixtures. On the other hand, we find different ordering of water molecules as determined from water's bending mode vibrations: Our SFG and MD simulation data show that the difference of excess mixing properties also propagates to the interfacial structure of the one to two topmost layers of the binary mixtures; reduced (enhanced) intermolecular interactions and accelerated (reduced) evaporation rates relative to ideal evaporation are linked with a lesser (greater) surface reorganization of the interfacial water molecules. The bending mode provides us new information about the complex interfacial structure, which paves a path for understanding evaporation and condensation processes, and ultimately perhaps a pathway toward controlling evaporation processes.

https://doi.org/10.1021/acs.jpcb.1c06001
J. Phys. Chem. B 2021, 125, 10639–10646

■ ASSOCIATED CONTENT

Supporting Information

The Supporting Information is available free of charge at https://pubs.acs.org/doi/10.1021/acs.jpcb.1c06001.

Evaporation measurement details, all SFG spectra and fitting procedures, estimation of HOD mole fraction, and MD simulation details (PDF)

■ AUTHOR INFORMATION

Corresponding Authors

Mischa Bonn − *Max Planck Institute for Polymer Research, 55128 Mainz, Germany;* orcid.org/0000-0001-6851-8453; Phone: +49 6131 379-161; Email: bonn@mpip-mainz.mpg.de

Yuki Nagata − *Max Planck Institute for Polymer Research, 55128 Mainz, Germany;* orcid.org/0000-0001-9727-6641; Phone: +49 6131 379-380; Email: nagata@mpip-mainz.mpg.de

Authors

Xiaoqing Yu − *Max Planck Institute for Polymer Research, 55128 Mainz, Germany*

Takakazu Seki − *Max Planck Institute for Polymer Research, 55128 Mainz, Germany;* orcid.org/0000-0002-3999-2313

Chun-Chieh Yu − *Max Planck Institute for Polymer Research, 55128 Mainz, Germany*

Kai Zhong − *University of Groningen, Zernike Institute for Advanced Materials, 9747 AG Groningen, The Netherlands*

Shumei Sun − *Department of Physics, Applied Optics Beijing Area Major Laboratory, Beijing Normal University, 100875 Beijing, China*

Masanari Okuno − *Department of Basic Science, Graduate School of Arts and Sciences, The University of Tokyo, Meguro 153-8902 Tokyo, Japan;* orcid.org/0000-0002-3682-9350

Ellen H. G. Backus − *Max Planck Institute for Polymer Research, 55128 Mainz, Germany; Department of Physical Chemistry, University of Vienna, 1090 Vienna, Austria;* orcid.org/0000-0002-6202-0280

Johannes Hunger − *Max Planck Institute for Polymer Research, 55128 Mainz, Germany;* orcid.org/0000-0002-4419-5220

Complete contact information is available at: https://pubs.acs.org/10.1021/acs.jpcb.1c06001

Author Contributions

#X.Y. and T.S. contributed equally.

Funding

Open access funded by Max Planck Society.

Notes

The authors declare no competing financial interest.

■ ACKNOWLEDGMENTS

We thank Maksim Grechko for fruitful discussions. We are grateful for the financial support from the MaxWater Initiative of the Max Planck Society. We acknowledge the financial support from the DAAD (Deutscher Akademischer Austauschdienst) Project Based Personnel Exchange Program (#57526761). J.H. acknowledges funding from the European Research Council (ERC) under the European Union's Horizon 2020 research and innovation program (grant agreement no. 714691). X.Y. thanks China Scholarship Council for the support.

■ REFERENCES

(1) de With, G. *Liquid-State Physical Chemistry: Fundamentals, Modeling, and Applications*; Wiley-VCH: 2013.

(2) Atkins, P.; de Paula, J. *Physical Chemistry*, 8th ed.; Oxford Univ. Press: 2006.

(3) Sommer, T.; Trejbal, J.; Kopecký, D. Isobaric and Isothermal Vapor-Liquid Equilibria for the Binary System of Water + Formic Acid at 99.41 KPa, 388.15 K, and 398.15 K. *J. Chem. Eng. Data* **2016**, *61*, 3398−3405.

(4) Kurihara, K.; Minoura, T.; Takeda, K.; Kojima, K. Isothermal Vapor-Liquid Equilibria for Methanol + Ethanol + Water, Methanol + Water, and Ethanol + Water. *J. Chem. Eng. Data* **1995**, *40*, 679−684.

(5) Lei, Z.; Li, C.; Chen, B. Extractive Distillation: A Review. *Sep. Purif. Rev.* **2003**, *32*, 121−213.

(6) Carey, J. S.; Lewis, W. K. Studies in Distillation. *Ind. Eng. Chem.* **1932**, *24*, 882−883.

(7) Jimenez, J. L.; Canagaratna, M. R.; Donahue, N. M.; Prevot, A. S. H.; Zhang, Q.; Kroll, J. H.; DeCarlo, P. F.; Allan, J. D.; Coe, H.; Ng, N. L.; et al. Evolution of Organic Aerosols in the Atmosphere. *Science* **2009**, *326*, 1525−1529.

(8) Shiraiwa, M.; Ammann, M.; Koop, T.; Pöschl, U. Gas Uptake and Chemical Aging of Semisolid Organic Aerosol Particles. *Proc. Natl. Acad. Sci. U. S. A.* **2011**, *108*, 11003−11008.

(9) Bones, D. L.; Reid, J. P.; Lienhard, D. M.; Krieger, U. K. Comparing the Mechanism of Water Condensation and Evaporation in Glassy Aerosol. *Proc. Natl. Acad. Sci. U. S. A.* **2012**, *109*, 11613−11618.

(10) Davies, J. F.; Miles, R. E. H.; Haddrell, A. E.; Reid, J. P. Influence of Organic Films on the Evaporation and Condensation of Water in Aerosol. *Proc. Natl. Acad. Sci. U. S. A.* **2013**, *110*, 8807−8812.

(11) Lu, Z.; Kinefuchi, I.; Wilke, K. L.; Vaartstra, G.; Wang, E. N. A Unified Relationship for Evaporation Kinetics at Low Mach Numbers. *Nat. Commun.* **2019**, *10*, 2368.

(12) Nagata, Y.; Usui, K.; Bonn, M. Molecular Mechanism of Water Evaporation. *Phys. Rev. Lett.* **2015**, *115*, 236102.

(13) O'Hare, K. D.; Spedding, P. L.; Grimshaw, J. Evaporation of the Ethanol and Water Components Comprising a Binary Liquid Mixture. *Dev. Chem. Eng. Miner. Process.* **1993**, *1*, 118−128.

(14) O'Hare, K. D. D.; Spedding, P. L. L. Evaporation of a Binary Liquid Mixture. *Chem. Eng. J.* **1992**, *48*, 1−9.

(15) Mackay, D.; Van Wesenbeeck, I. Correlation of Chemical Evaporation Rate with Vapor Pressure. *Environ. Sci. Technol.* **2014**, *48*, 10259−10263.

(16) Varilly, P.; Chandler, D. Water Evaporation: A Transition Path Sampling Study. *J. Phys. Chem. B* **2013**, *117*, 1419−1428.

(17) Shen, Y. R.; Ostroverkhov, V. Sum-Frequency Vibrational Spectroscopy on Water Interfaces: Polar Orientation of Water Molecules at Interfaces. *Chem. Rev.* **2006**, *106*, 1140−1154.

(18) Bonn, M.; Nagata, Y.; Backus, E. H. G. Molecular Structure and Dynamics of Water at the Water-Air Interface Studied with Surface-Specific Vibrational Spectroscopy. *Angew. Chem., Int. Ed.* **2015**, *54*, 5560−5576.

(19) Chen, H.; Gan, W.; Lu, R.; Guo, Y.; Wang, H. Determination of Structure and Energetics for Gibbs Surface Adsorption Layers of Binary Liquid Mixture 2. Methanol + Water. *J. Phys. Chem. B* **2005**, *109*, 8064−8075.

(20) Lu, R.; Gan, W.; Wu, B. H.; Zhang, Z.; Guo, Y.; Wang, H. F. C-H Stretching Vibrations of Methyl, Methylene and Methine Groups at the Vapor/Alcohol (n = 1−8) Interfaces. *J. Phys. Chem. B* **2005**, *109*, 14118−14129.

(21) Sung, J.; Park, K.; Kim, D. Surfaces of Alcohol - Water Mixtures Studied by Sum-Frequency Generation Vibrational Spectroscopy. *J. Phys. Chem. B* **2005**, *109*, 18507−18514.

(22) Ishihara, T.; Ishiyama, T.; Morita, A. Surface Structure of Methanol/Water Solutions via Sum Frequency Orientational Analysis and Molecular Dynamics Simulation. *J. Phys. Chem. C* **2015**, *119*, 9879−9889.
(23) Ishiyama, T.; Takagi, S.; Hirano, T.; Wang, L.; Morita, A. Comment on "Toward Unraveling the Puzzle of Sum Frequency Effects of Concentration-Dependent Hyperpolarizability. *J. Phys. Chem. C* **2020**, *124*, 25160.
(24) Stanners, C. D.; Du, Q.; Chin, R. P.; Cremer, P.; Somorjai, G. A.; Shen, Y. R. Polar Ordering at the Liquid-Vapor Interface of n-Alcohols (C1-C8). *Chem. Phys. Lett.* **1995**, *232*, 407−413.
(25) Kirschner, J.; Gomes, A. H. A.; Marinho, R. R. T.; Björneholm, O.; Ågren, H.; Carravetta, V.; Ottosson, N.; De Brito, A. N.; Bakker, H. J. The Molecular Structure of the Surface of Water-Ethanol Mixtures. *Phys. Chem. Chem. Phys.* **2021**, *23*, 11568−11578.
(26) Johnson, C. M.; Tyrode, E.; Kumpulainen, A.; Leygraf, C. Vibrational Sum Frequency Spectroscopy Study of the Liquid/Vapor Interface of Formic Acid/Water Solutions. *J. Phys. Chem. C* **2009**, *113*, 13209−13218.
(27) Seki, T.; Yu, C.-C.; Yu, X.; Ohto, T.; Sun, S.; Meister, K.; Backus, E.; Bonn, M.; Nagata, Y. Decoding Molecular Water Structure at Complex Interfaces through Surface-Specific Spectroscopy of the Water Bending Mode. *Phys. Chem. Chem. Phys.* **2020**, *22*, 10934−10940.
(28) Seki, T.; Sun, S.; Zhong, K.; Yu, C. C.; Machel, K.; Dreier, L. B.; Backus, E. H. G.; Bonn, M.; Nagata, Y. Unveiling Heterogeneity of Interfacial Water through the Water Bending Mode. *J. Phys. Chem. Lett.* **2019**, *10*, 6936−6941.
(29) Nitsche, M.; Gbadamosi, R. *Practical Column Design Guide*; Springer: 2017.
(30) Abraham, M. J.; Murtola, T.; Schulz, R.; Páll, S.; Smith, J. C.; Hess, B.; Lindahl, E. GROMACS: High Performance Molecular Simulations through Multi-Level Parallelism from Laptops to Supercomputers. *SoftwareX* **2015**, *2*, 19−25.
(31) Jorgensen, W. L.; Maxwell, D. S.; Tirado-Rives, J. Development and Testing of the OPLS All-Atom Force Field on Conformational Energetics and Properties of Organic Liquids. *J. Am. Chem. Soc.* **1996**, *118*, 11225−11236.
(32) Abascal, J. L. F.; Vega, C. A General Purpose Model for the Condensed Phases of Water: TIP4P/2005. *J. Chem. Phys.* **2005**, *123*, 234505.
(33) Ohto, T.; Backus, E. H. G.; Mizukami, W.; Hunger, J.; Bonn, M.; Nagata, Y. Unveiling the Amphiphilic Nature of TMAO by Vibrational Sum Frequency Generation Spectroscopy. *J. Phys. Chem. C* **2016**, *120*, 17435−17443.
(34) Wang, C.; Groenzin, H.; Shultz, M. J. Surface Characterization of Nanoscale TiO_2 Film by Sum Frequency Generation Using Methanol as a Molecular Probe. *J. Phys. Chem. B* **2004**, *108*, 265−272.
(35) Ohto, T.; Hunger, J.; Backus, E. H. G.; Mizukami, W.; Bonn, M.; Nagata, Y. Trimethylamine-N-Oxide: Its Hydration Structure, Surface Activity, and Biological Function, Viewed by Vibrational Spectroscopy and Molecular Dynamics Simulations. *Phys. Chem. Chem. Phys.* **2017**, *19*, 6909−6920.
(36) Hou, J.; Zhang, X.; Lu, Z. Comparing Vibrational Sum Frequency Generation Responses at Fused Silica and Fluorite/Liquid Ethanol Interfaces. *Chem. Phys.* **2020**, *536*, 110814.
(37) Marushkevich, K.; Khriachtchev, L.; Räsänen, M. Hydrogen Bonding between Formic Acid and Water: Complete Stabilization of the Intrinsically Unstable Conformer. *J. Phys. Chem. A* **2007**, *111*, 2040−2042.
(38) Wolfrum, K.; Graener, H.; Laubereau, A. Sum-Frequency Vibrational Spectroscopy at the Liquid-Air Interface of Methanol/Water Solutions. *Chem. Phys. Lett.* **1993**, *213*, 41−46.
(39) Ma, G.; Allen, H. C. Surface Studies of Aqueous Methanol Solutions by Vibrational Broad Bandwidth Sum Frequency Generation Spectroscopy. *J. Phys. Chem. B* **2003**, *107*, 6343−6349.
(40) Li, X.; Liu, J.; Lin, K.; Zhang, Y.; Zhang, Y.; Zheng, R.; Shi, Q.; Guo, Y.; Lu, Z. Toward Unraveling the Puzzle of Sum Frequency Generation Spectra at Interface of Aqueous Methanol Solution: Effects of Concentration-Dependent Hyperpolarizability. *J. Phys. Chem. C* **2019**, *123*, 12975−12983.
(41) Du, Q.; Superfine, R.; Freysz, E.; Shen, Y. R. Vibrational Spectroscopy of Water at the Vapor/Water Interface. *Phys. Rev. Lett.* **1993**, *70*, 2313−2316.
(42) Ju, S.; Wu, T.-D.; Yeh, Y.-L.; Wei, T.-H.; Huang, J.-Y.; Lin, S. H. Sum Frequency Vibrational Spectroscopy of the Liquid-Air Interface of Aqueous Solutions of Ethanol in the OH Region. *J. Chin. Chem. Soc.* **2001**, *48*, 625−629.
(43) Schaefer, J.; Backus, E. H. G.; Nagata, Y.; Bonn, M. Both Inter- and Intramolecular Coupling of O-H Groups Determine the Vibrational Response of the Water/Air Interface. *J. Phys. Chem. Lett.* **2016**, *7*, 4591−4595.
(44) Yu, C.-C.; Chang, K.-Y.; Masanari, O.; Seki, T.; Ohto, T.; Yu, X.; Zhong, K.; Korepanov, V.; Hamaguchi, H.; Bonn, M.; et al. Vibrational Couplings and Energy Transfer Pathways of Water's Bending Mode. *Nat. Commun.* **2020**, *11*, 5977.
(45) Seki, T.; Yu, C.-C.; Chiang, K.-Y.; Tan, J.; Sun, S.; Ye, S.; Bonn, M.; Nagata, Y. Disentangling Sum-Frequency Generation Spectra of the Water Bending Mode at Charged Aqueous Interfaces. *J. Phys. Chem. B* **2021**, *125*, 7060−7067.
(46) Vinaykin, M.; Benderskii, A. V. Vibrational Sum-Frequency Spectrum of the Water Bend at the Air/Water Interface. *J. Phys. Chem. Lett.* **2012**, *3*, 3348−3352.
(47) Nagata, Y.; Hsieh, C.-S.; Hasegawa, T.; Voll, J.; Backus, E. H. G.; Bonn, M. Water Bending Mode at the Water−Vapor Interface Probed by Sum-Frequency Generation Spectroscopy: A Combined Molecular Dynamics Simulation and Experimental Study. *J. Phys. Chem. Lett.* **2013**, *4*, 1872−1877.
(48) Dutta, C.; Benderskii, A. V. On the Assignment of the Vibrational Spectrum of the Water Bend at the Air/Water Interface. *J. Phys. Chem. Lett.* **2017**, *8*, 801−804.
(49) Pettersson, M.; Lundell, J.; Khriachtchev, L. IR Spectrum of the Other Rotamer of Formic Acid, Cis-HCOOH. *J. Am. Chem. Soc.* **1997**, *119*, 11715−11716.
(50) Redington, R. L. Vibrational Spectra and Normal Coordinate Analysis of Isotopically Labeled Formic Acid Monomers. *J. Mol. Spectrosc.* **1977**, *65*, 171−189.
(51) Millikan, R. C.; Pitzer, K. S. Infrared Spectra and Vibrational Assignment of Monomeric Formic Acid. *J. Chem. Phys.* **1957**, *27*, 1305.
(52) Tomlinson, G. E.; Gurnutte, B.; Hathaway, C. E. Temperature Dependence of the Raman and Infrared Spectrum of Liquid Formic Acid I. *J. Mol. Spectrosc.* **1970**, *36*, 26−33.
(53) Millikan, R. C.; Pitzer, K. S.; Millikan, B. R. C.; Pitzer, K. S.; Millikan, R. C. The Infrared Spectra of Dimeric and Crystalline Formic Acid. *J. Am. Chem. Soc.* **1958**, *80*, 3515−3521.
(54) Gadermann, M.; Vollmar, D.; Signorell, R. Infrared Spectroscopy of Acetic Acid and Formic Acid Aerosols: Pure and Compound Acid/Ice Particles. *Phys. Chem. Chem. Phys.* **2007**, *9*, 4535−4544.

https://doi.org/10.1021/acs.jpcb.1c06001
J. Phys. Chem. B 2021, 125, 10639−10646